International journal of imaging science and engineering

ISSN: 1934--9955 www.ijise.net

Vol-20 Issue-01 Mar 2025

Replacing the Grid Interface Transformer in Wind Energy Conversion System With Solid-State Transformer

Ms. Balagani Jhansi Rani[1] , Mr. Keshavarapu ShivaKrishna[2]

[1]Asst.professor, Department of Electrical & Electronics Engineering, Mallareddy College of Engineering & Technology, Hyderabad, T.G, India.

[2]Asst.professor, Department of Electrical & Electronics Engineering, St.Martins Engineering College Hyderabad, T.G, India.

***Abstract*—In wind energy conversion systems, the fundamental frequency step-up transformer acts as a key interface between the wind turbine and the grid. Recently, there have been efforts to replace this transformer by an advanced power-electronics-based solid-state transformer (SST). This paper proposes a configuration that combines the doubly fed induction generator-based wind tur- bine and SST operation. The main objective of the proposed con- figuration is to interface the turbine with the grid while providing enhanced operation and performance. In this paper, SST controls the active power to/from the rotor side converter, thus, eliminating the grid side converter. The proposed system meets the recent grid code requirements of wind turbine operation under fault condi- tions. Additionally, it has the ability to supply reactive power to the grid when the wind generation is not up to its rated value. A detailed simulation study is conducted to validate the performance of the proposed configuration.**

***Index Terms*—Doubly fed induction generator, fault ride through, power electronic transformer, solid-state transformer.**

I. INTRODUCTION

OVER the last decade, the penetration of renewable energy sources has been increasing steadily in the power system. In particular, wind energy installations have grown rapidly with global installed capacity increasing from 47.6 GW in 2004 to 369.6 GW in 2014 [1]. Amongst the many technologies that exist for wind energy conversion systems (WECS), doubly fed induction generators (DFIG) have been prevalent due to variable speed operation, high power density and lower cost [2], [3]. DFIG based WECS consist of an induction generator whose stator is directly connected to the grid while its rotor is connected via back to back converters known as the rotor side converter (RSC) and grid side converter (GSC), respectively [3]. The gen- erator is normally operated at a range of 500 V–700 V and is connected to the transmission network (11–33 kV) through a transformer that acts as an integral part of the WECS to interface the wind turbine and the grid.

Recently, there has been much interest in developing an al- ternative to the traditional fundamental frequency transformer using solid-state devices.

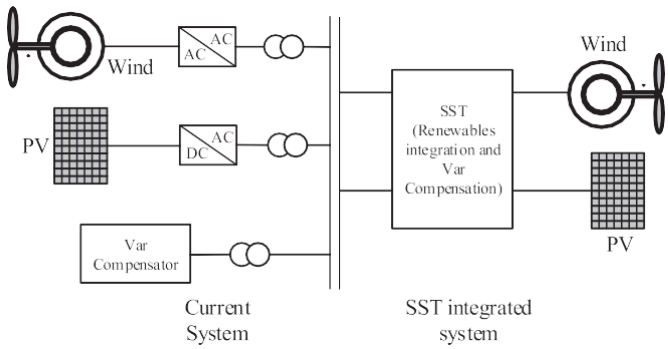

Fig. 1 Expected SST integrated grid.

The solid-state transformer (SST) achieves voltage conver- sion through a series of power electronics devices while offer- ing multiple advantages, such as, smaller size, improved power quality and fault tolerant features [4]–[11].

Fig. 1 shows a power distribution system based on SST as envisioned in [4]. Proposed in 1980 [5], advances in solid-state technology have made SST more viable today leading to in- creased research in its feasibility and physical realization.

A promising 10 kVA prototype has been developed and pre- sented in [6]. Further, the use of high voltage silicon carbide (SiC) power devices for SST has been explored and presented in [7], [8]. As seen in Fig. 1, SST can act as an interface between the grid

International journal of imaging science and engineering
ISSN: 1934--9955 www.ijise.net
Vol-20 Issue-01 Mar 2025

and generation sources. However, research showing detailed configurations for integrating existing technologies is limited. In [9], work is reported on using SST in a microgrid based on renewable sources. In [10], SST is used to interface a wind park based on squirrel cage induction generator (SCIG) with the grid. However, a detailed analysis on fault ride through requirement and reactive power support has not been conducted in [10].

In this paper, a new configuration is proposed that combines the operation of DFIG based WECS and SST. This configu- ration acts as an interface between the wind turbine and grid while eliminating the GSC of DFIG. Moreover, it is essen- tial to have fault ride through (FRT) incorporated in DFIG system to meet the grid code requirements [11]–[20]. In the proposed work, the developed configuration allows DFIG to ride through faults seamlessly, which is the aspect (FRT) that has not been addressed in the earlier work on SST interfaced WECS.

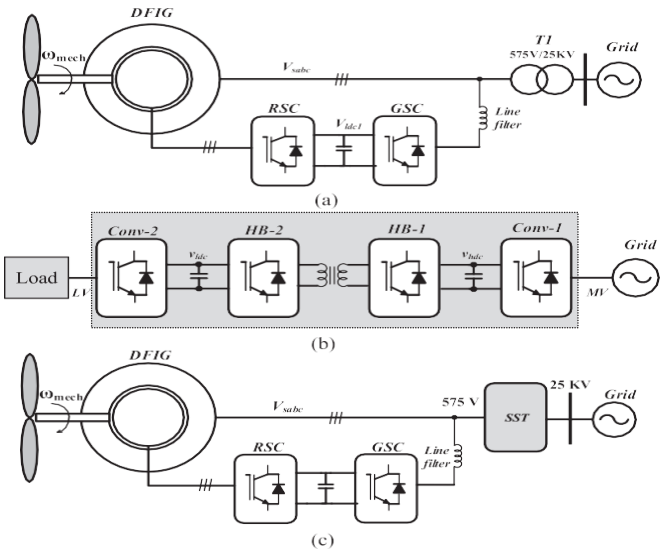

Fig. 2 (a) Regular DFIG configuration, (b) SST structure and (c) configuration suggested in [10].

II. Proposed System Configuration and Modeling

A. Motivation for DFIG

In [21], it has been reported that a DFIG based wind turbine is the lightest amongst the current wind systems which also explains its wide commercial use. Moreover, in the proposed configuration, the GSC present in traditional DFIG systems is removed making the machine setup further lighter. On the other hand, SST being used in an AC/AC system is expected to be 25% smaller in volume than traditional low frequency transformer [22]. Thus, the use of SST to interface a DFIG based wind system can be expected to provide further reduction in weight and volume when compared to other wind systems with the fundamental frequency transformer.

B. Background

The widely used DFIG based WECS configuration is shown in Fig. 2(a). The stator terminals of the machine are connected directly to the grid while the rotor terminals are connected via back to back converters. The RSC allows for variable speed operation of the machine by injecting or drawing active power from the rotor. The GSC maintains the DC link by transferring the active power from the rotor to the grid or vice versa. The step up transformer T1, is the interface between the DFIG system and grid.

Three stage SST configuration is shown in Fig. 2(b), where it connects the grid to a distribution load. Conv-1 is a fully controlled three-phase converter connected to the high voltage grid (11–33 kV). It draws real power from the grid and main- tains the high voltage DC bus (v_{hdc}). This high voltage DC is converted to high frequency AC voltage by a half bridge con- verter (HB-1) which is then stepped down using a smaller sized high frequency transformer. This transformer provides the gal- vanic isolation between the grid and load. A second half bridge converter (HB−2) converts the low voltage AC to low voltage DC voltage (v_{ldc}). This DC bus supports conv-2 which main- tains the three-phase/single phase supply voltage to the load by producing a controlled three phase voltage. The configuration thus performs the function of a regular transformer allowing for bi-directional power flow using a series of power electronics devices [5]–[10].

International journal of imaging science and engineering
ISSN: 1934--9955 www.ijise.net
Vol-20 Issue-01 Mar 2025

As mentioned earlier, the use of SST in WECS has been ex- plored by Xu *et al.* in [10]. SST was used in an SCIG based WECS replacing the step-up transformer between the turbine and grid. It was shown that SST can improve the voltage profile at the terminals of the SCIG. While the focus of [10] was on SCIG, possible configuration for DFIG systems was also show- cased that is represented in Fig. 2(c). The step-up transformer T1 in Fig. 2(a) is directly replaced by the SST in Fig. 2(c).

C. Proposed System Description

The general DFIG based WECS representation is shown in Fig. 3(a) whereas the proposed system configuration is shown in Fig. 3(b). In the proposed configuration, the fundamental frequency transformer is replaced by the SST. The proper control of SST converter that is close to the stator of DFIG, addressed as machine interfacing converter (MIC), can aid the machine in its operation. Thus, it is proposed to eliminate the GSC in the DFIG system configuration by incorporating its role in SST. Note that this new arrangement modifies the overall operation and control of standard GSC-RSC based DFIG system. In principle, the machine terminal voltages can be maintained constant in spite of any voltage variations in the grid using MIC.

The direction of power flow in the proposed configuration occurs from the low voltage machine terminals to the grid. The MIC is responsible for: (*i*) maintaining the required voltages at the stator terminals and (*ii*) transferring the real power from the stator terminals (P_s) to the low voltage DC bus (v_{ldc}). This low voltage DC bus is regulated by the high frequency stage con- verters (HB1 and HB2) and not by the DFIG. In other words, MIC acts as a stiff grid at the stator terminals. Interestingly, the low voltage DC bus (magnitude) is very close to the one controlled by GSC in the regular DFIG configuration [v_{ldc1} in Fig. 2(a)]. This allows the RSC in the proposed configura- tion to be connected directly to v_{ldc} of SST. The v_{ldc} has two functions, namely, (*i*) to transfer active power from the sta- tor terminals to the grid and (*ii*) to transfer active power (P_r) to/from the RSC during sub-synchronous or super-synchronous operation.

The power transfer through the high frequency stage, from the low voltage DC bus to the high voltage DC bus (v_{hdc}), is controlled by introducing a phase shift between the two high frequency AC voltages with the objective of regulating the DC bus voltage (v_{ldc}). The grid interfacing converter (GIC) connects SST to the grid and maintains the DC link (v_{hdc}) by exchanging active power with the grid.

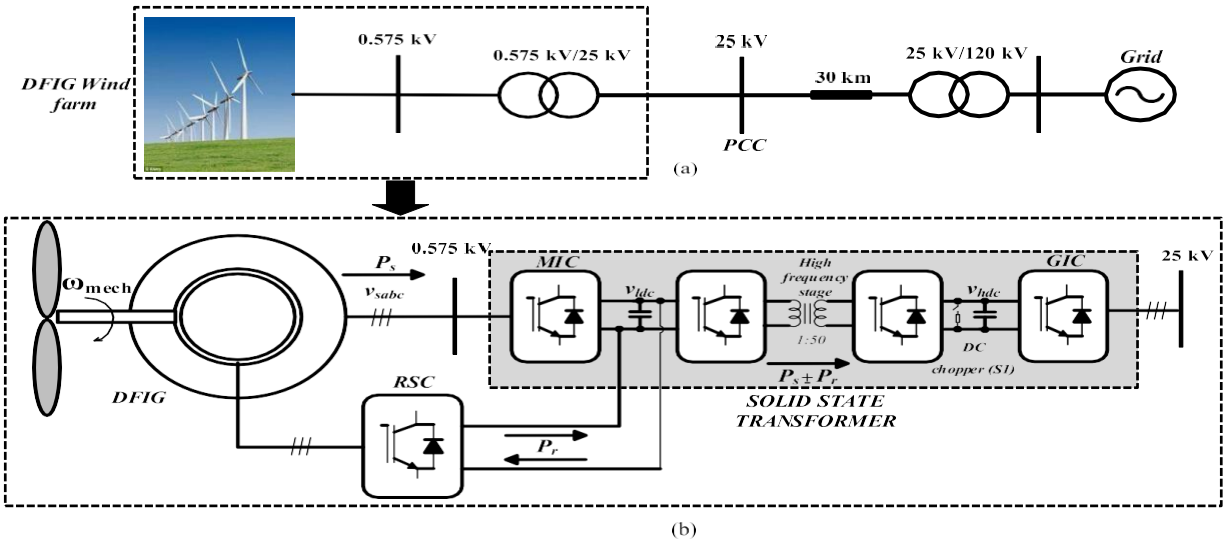

Fig. 3. (a) Regular DFIG configuration and (b) Proposed SST based DFIG configuration.

To provide an effective FRT in the proposed configuration, a DC chopper is incorporated at v_{hdc} bus. During the grid fault conditions, the power being generated by the wind turbine is evacuated through the high frequency stage into the DC chopper. Further, the high frequency stage continues to maintain the low voltage DC bus (v_{ldc}), allowing the voltages at the machine terminals to be constant. The presence of GIC further helps to achieve the recent grid code requirements of reactive current injection without requiring any additional control or device. Furthermore, the GIC can provide reactive power support to the grid

International journal of imaging science and engineering
ISSN: 1934--9955 www.ijise.net
Vol-20 Issue-01 Mar 2025

during low wind generation periods.

D. DFIG Modeling

The DFIG is modeled using the $d-q$ synchronous reference frame rotating at synchronous speed as depicted in [4]. The machine flux equations can be written in the $d-q$ reference frame as,

$$\lambda_{sd} = L_{ls} i_{sd} + L_m (i_{sd} + i_{rd}) \quad \lambda_{sq} = L_{ls} i_{sq} + L_m (i_{sq} + i_{rq}) \quad \lambda_{rd} = L_{lr} i_{rd} + L_m (i_{sd} + i_{rd}) \quad (1)$$

$$\lambda_{rq} = L_{lr} i_{rq} + L_m (i_{sq} + i_{rq})$$

The voltage equations for the stator and rotor are given as,

$$v_{sqsd} = r_s i_{sd} - \omega\lambda_{sq} + \frac{d}{dt}\lambda_{sq}^{sd} \quad (2)$$

$$v_{rd} = r_r i_{rd} - (\omega - \omega_r)\lambda_{rq} + \frac{d}{dt}\lambda \quad v_{rq} = r_r i_{rq} + (\omega - \omega_r)\lambda_{rd} + \frac{d\lambda}{dt}_{rq}$$

The d and q axes quantities are represented by the respective subscripts d and q. r_s and r_r represent the stator and rotor resistances. L_{ls} , L_{lr} and L_m represent the stator, rotor and mutual inductances referred to stator. ω represents the electrical supply frequency and ω_r represents the rotor frequency. Using (1),(2), the torque equation for the machine can be obtained as,

$$T = -\frac{\lambda_{sd} L_m}{L_s} i_{qr} \quad (3)$$

It can be understood from the above equation that on aligning the stator flux with the d-axis, the torque in the machine can be controlled by varying i_{qr}. This is the basis on which the rotor side converter is controlled. It can also be shown that by varying i_{dr}, reactive power output from the stator can be controlled. Further details on the DFIG modeling can be obtained from [4].

III. Control of the Proposed System

To ensure smooth operation of the proposed configuration, the control objectives and algorithms for the RSC, MIC and the GIC are discussed below and shown in Fig. 4.

A. RSC Control

The rotor side control ensures the variable speed operation of DFIG by enabling the generator to work in super synchronous or sub synchronous modes. In super synchronous mode, the total power generated is partially evacuated through the RSC. Under sub synchronous modes, the RSC injects active power into the rotor. The RSC in the proposed converter is controlled using a decoupled $d-q$ synchronous frame reference. The q- axis of the reference frame is aligned with the machine stator voltage. On doing this, as per (3), the torque produced by the machine can be directly controlled by controlling the q-axis rotor current i_{qr}. Moreover, the reactive power produced at the stator terminal can also be controlled by controlling the d-axis

International journal of imaging science and engineering
ISSN: 1934--9955 www.ijise.net
Vol-20 Issue-01 Mar 2025

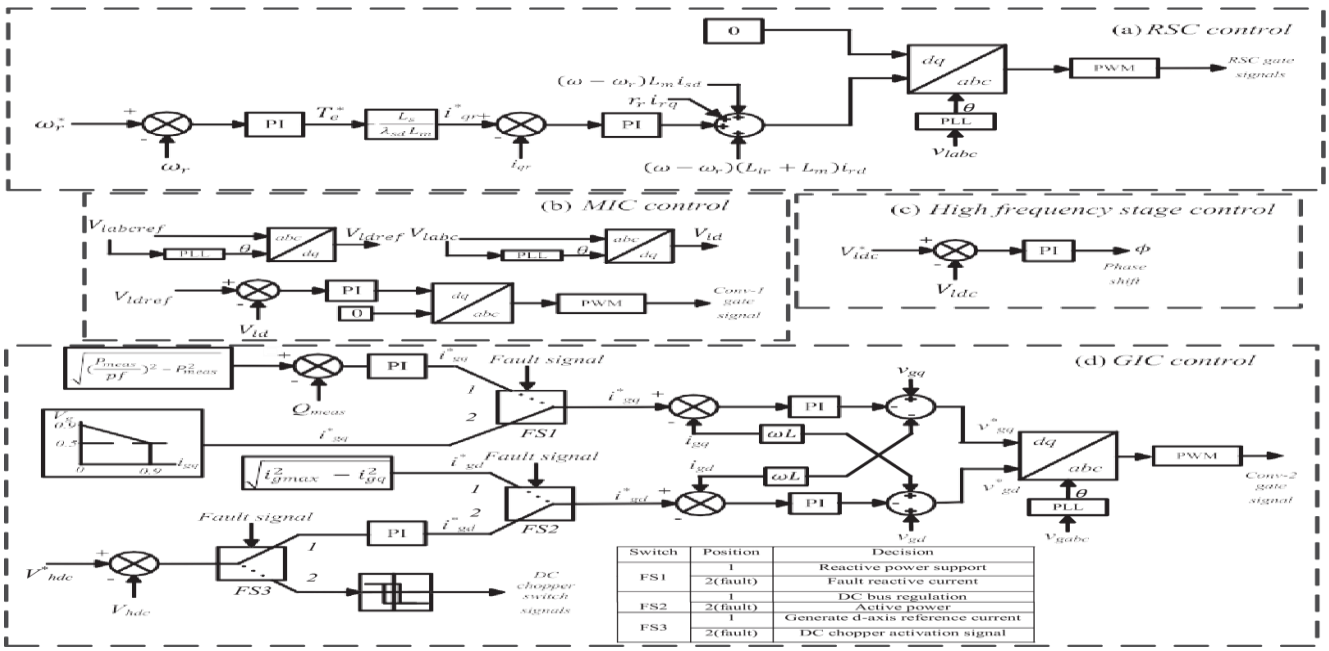

Fig. 4. Control diagram of proposed configuration.

rotor current i_{dr}. The control schematic for the same is shown in Fig. 4. A suitable MPPT curve is used to track the optimal rotor speed and is compared with the measured rotor speed. The error is processed by a PI controller to produce the reference torque (T^*) for the machine. Using (3), the rotor q-axis reference current (i^{e*}_{qr}) is calculated. This current is compared with the actual rotor q-axis current (i_{qr}) and the error is processed by a PI controller to generate the q-axis reference voltage (v^*_{qr}). In the proposed configuration, the stator terminals are completely decoupled from the grid through the SST. The GIC supplies any reactive power requirement from the grid and the machine only generates active power. This eliminates the need for control over the d-axis rotor current and voltage. Thus, the d-axis rotor voltage reference for RSC (v^*_{dr}) is maintained as zero. The $d-q$ axis reference voltages are then converted to three phase and used to generate the gate pulses for the RSC. Further details regarding the control system can be obtained in [4].

B. MIC Control

The MIC is the first stage of the SST connecting the low volt- age machine output to the high frequency stage. This converter is controlled to maintain 1 p.u. voltage (0.575 kV) at 50 Hz at the stator terminals of the machine.

The control is achieved by generating a reference voltage and comparing the d-axis component of the reference (v_{sd}^*) with the voltage at the output of the converter (v_{sd}). The power generated at the stator terminals of the machine is thus absorbed by the low voltage DC bus connected to MIC operating at 1.15 kV.

C. High Frequency Stage Control

The high frequency stage transforms the low voltage DC bus voltage (1.15 kV) into high voltage DC (50 kV). The DC voltages are converted into high frequency AC voltages by the two half bridge converters. Power is transferred by introducing a phase shift between the AC voltages of the two converters linked together by a high frequency transformer. The equation that governs the transfer of power is given as,

$$P = \frac{v_{hdc} v_{ldc}\, \varphi(\pi - \varphi)}{2\pi\omega L_k \pi} \quad (4)$$

where φ is the phase shift between the AC voltages and L_k is the leakage inductance of the high frequency transformer. The complete derivation of the power transfer equation and further details can be obtained in [23]–[25].

International journal of imaging science and engineering
ISSN: 1934--9955 www.ijise.net
Vol-20 Issue-01 Mar 2025

The control objective of high frequency stage, in the proposed configuration, is to maintain the low voltage DC bus voltage (v_{ldc}) at a constant level. In order to achieve this, the reference voltage v^*_{ldc} is compared with the measured value and the resulting error is processed by a PI controller which produces the required phase shift φ that transfers the active power from the low voltage DC bus to the high voltage DC bus. The schematic for control is shown in Fig. 4(c).

D. GIC Control

While the control of other converters remains the same in fault and normal conditions, GIC is controlled differently during fault conditions. The control and operation of GIC is discussed in two modes. Fault detection switches are used that are triggered when a fault is detected. The positions of the switches and their operation are summarized in a table in Fig. 4(d).

1) Normal Mode: Under normal mode of operation, the ob- jective of the GIC is to ensure that the active power produced by the wind system is delivered to the grid. Additionally, it is sug- gested in this paper that the GIC provide reactive support as per user defined power factor to the grid when the wind generation is lower than rated value. Fig. 4(d) shows the overall control of GIC.

The control of the converter is designed based on the $d-q$ reference frame. The d-axis current (i_{gd}) controls the flow of active power and the DC bus voltage while the q-axis current (i_{gq}) controls the reactive power flow. The q-axis reference grid current (i^*_{gq}) is generated based on the user defined power factor requirement which is used to calculate the reference reactive power (Q^*) which is compared with the measured reactive power (Q_{meas}) and passed through a PI controller. Reference reactive power Q^* can be calculated from the power factor as

$$Q_* = \sqrt{\left(\frac{P_{meas}}{pf}\right)^2 - P_{meas}^2} \qquad (5)$$

The d-axis reference current is generated by passing the er- ror between the measured DC bus voltage and its reference through a PI controller. An outer loop voltage controller then generates the d-axis reference voltage v^*_{gd}. Similarly, the q-axis reference voltage v^*_{gq} is obtained from a PI controller on the q-axis current.

2) Fault Mode: The objective of the GIC under fault con- ditions is to supply the reactive currents as per the grid codes. The fault in the system is identified by monitoring the positive sequence grid voltage which is effective in both symmetrical and unsymmetrical fault conditions.

Upon identifying the fault, the fault switches (FS1 to FS3) shown in Fig. 4(d) are activated. Under fault conditions, preference is given to reactive current injection and the control of DC bus by the GIC is deactivated by FS3. The reactive current reference enabled by FS2 for the GIC is generated as per the

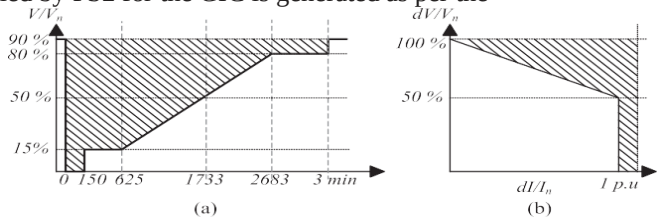

Fig. 5. Latest FRT grid code requirements (a) The Fault Ride Through re- quirement and (b) The reactive current requirement.

grid codes in [19] and [20] shown in Fig. 5 and is calculated as,

$$\frac{\Delta i}{i_n} = \begin{cases} \frac{\Delta_n v}{1} * 1 & \text{if } 1 > \frac{\Delta_n v}{v_n} > 0.5 \\ i_{*gq} \frac{v}{0.5} & \text{if } 0.5 > \frac{\Delta v}{v_n} > 0 \end{cases}$$

International journal of imaging science and engineering
ISSN: 1934--9955 www.ijise.net
Vol-20 Issue-01 Mar 2025

(6)

where Δv, is the difference between the pre-fault voltage and the current grid voltage and v_n is the rated nominal voltage. Δi is the difference between the pre-fault reactive current and the reactive current during fault and i_n is the rated current value. In the case considered in this paper i_n is 1 p.u. and there is no pre-fault reactive current, thus, $\frac{\Delta i}{i_n}$ is equal to the reactive current to be injected i.e. i^*_{gq} .

Recent grid codes in some countries have even more aggres- sive reactive current requirements sometimes requiring the wind farm to supply up to 1.2 p.u. reactive currents [26]. The q-axis reference current is then compared with the measured one. The error is processed by a PI controller to generate the q-axis refer- ence voltage (v_{qr^*}). When the fault is less severe and the voltage dip is less than 1 p.u. the grid codes do not impose any restriction on injecting active power into the grid. Hence, after prioritizing reactive current injection, the remaining capacity of the GIC is used to continue to inject any active power possible by switching FS1. The reference for the d-axis current is generated as follows based on the maximum allowable rating of the GIC, i and $_{gmax}$ is expressed as

$$i^*_{gd} = \sqrt{i^2_{gmax} - i^2_{gq}} \qquad (7)$$

Upon identification of fault, in order to prevent the DC bus voltage from rising, a DC chopper is employed (FS3 at position 2). The measured error between the high voltage DC bus reference (v^*_{hdc}) and the measured value (v_{hdc}) is passed through a hysteresis relay that produces the switching signal for DC chopper circuit. which is designed to allow for a two percent variation in bus voltage.

$$S1 = \begin{cases} \text{ON} & \text{if } v^*_{hdc} - v_{hdc} > 1 \text{ kV} \\ \text{OFF} & \text{if } v_{hdc^*} - v_{hdc} < 1 \text{ kV} \end{cases} \qquad (8)$$

IV. System Simulation and Analysis

To verify the effectiveness of the proposed configuration, detailed simulations are carried out. The simulated system is as represented in Fig. 3. A detailed model of proposed configuration is developed using the SIMULINK and SimPowerSystems toolbox in MATLAB. All the system param- eters are given in Table I. The performance of proposed system is evaluated under different operating conditions. All the results shown are in p.u. on a base of 5.1 MVA with respective voltages.

A. Normal Operation

Firstly, the operation of the proposed configuration is shown under normal grid conditions in Fig. 6. In this scenario (between 4.9 to 5 sec), the wind turbine is operated at a speed of $13 \cdot \mathrm{m/s}$ thus not producing peak power. The wind turbines produce a total of 4.2 MW active power. Like general DFIG, the system delivers this wind generated active power to the grid as shown in Fig. 6(e) through the SST.

That is, there is no reactive power support from the GIC. Figs. 6(a) and (b) show the grid voltages and currents at the output of the GIC. Figs. 6(c) and (d) give the stator terminal voltages and machine currents at 0.575 kV. The high and low voltage DC bus voltage profiles are illus- trated in Figs.6(f) and (g), respectively. Fig. 6(h) provides the controlled inner loop d-axis and q-axis currents of the GIC that control the active and reactive power injection into the grid, re- spectively. Fig. 6(i) shows the rotor speed of the machine which remains constant at 1.2 p.u.

International journal of imaging science and engineering
ISSN: 1934--9955 www.ijise.net
Vol-20 Issue-01 Mar 2025

B. Reactive Power Support During Steady-State

The feature of using the GIC capacity to provide reactive power support during lower wind speeds is also shown in Fig. 5 (between time interval of 5 sec to 5.1 sec). At 5 sec, the reactive power reference is activated to fully utilize the GIC capacity. With 13 · m/s wind speed (i.e. 4.2 MW), the proposed configuration can inject 2.7 MVar (Fig. 5(e)).

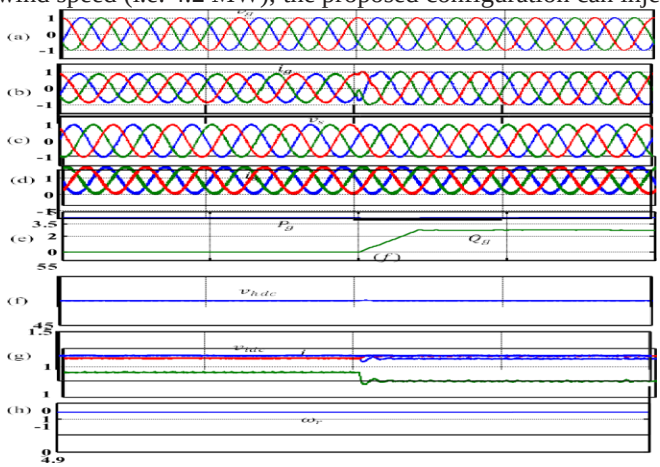

Fig 6. Normal operation of proposed configuration showing dynamics of P (i)and Q injection.

Further, as seen from Fig. 7(g), the DC chopper evac- uates the active power generated by the turbines successfully. Thus, in the proposed configuration, turbines seamlessly ride through the grid fault. On the grid side, the GIC is controlled to inject necessary reactive current to meet the grid codes. Fig. 7(e) shows the *d* and *q*-axis currents of the GIC, i_{gd} and i_{gq} , respectively. In pre-fault conditions it can be seen that i_{gd} is at 1 p.u. since the wind turbine is operated at maximum capacity. The *q*-axis current i_{gq} on the other hand is at zero as no reactive power is being injected. At 3 sec, when the fault occurs, the fault switch (FS2) is set to position 2 and the reactive current reference i^*_{gq} is calculated as per (6). The GIC, thus, injects 0.9 p.u. reactive current that can be seen in Fig. 7(e). The *d*-axis

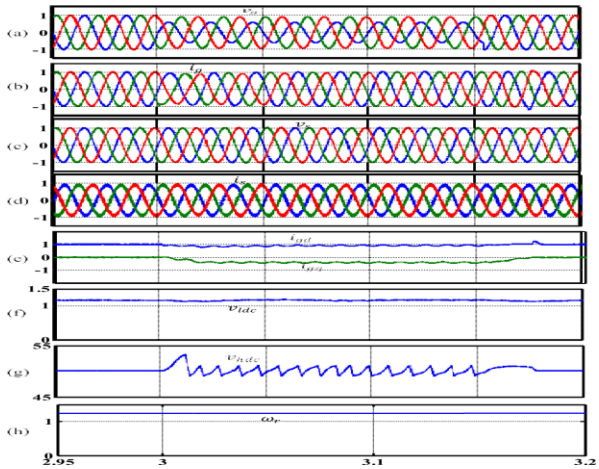

Fig 8. Performance of the proposed configuration under three-phase unsym- metrical L-G fault. (a) Grid voltages, (b) grid currents,(c) stator terminal volt- ages, (d) stator currents, (e) inner loop controlled axis grid currents, (f) low voltage DC bus (g) high voltage DC bus voltage and (h) rotor speed.

International journal of imaging science and engineering
ISSN: 1934--9955 www.ijise.net
Vol-20 Issue-01 Mar 2025

maximum power (15 m/s). Fig. 8(a) shows the grid volt- ages when the fault occurs at 3 sec and lasts for 150 ms. Fig. 8(b) shows the grid currents injected by the GIC. Note that the currents remain symmetrical despite the unsymmetrical fault. Figs. 8(c) and (d) show the stator voltages and currents which remain undisturbed as the MIC maintains rated stator voltages similar to the symmetrical case.

D. Unsymmetrical Fault Condition

The performance of the proposed configuration is tested un- der unsymmetrical faults condition as well. A single phase L-G fault is applied at the upstream grid when the DFIG is produc-

E. Comparison

In order to showcase the advantages of the proposed con- figuration, a comparison has been made in Fig. 9, of DFIG operation current (i_{gd})is calculated as per (7). and i_{gq} are shown in Fig. 8(e), respectively.

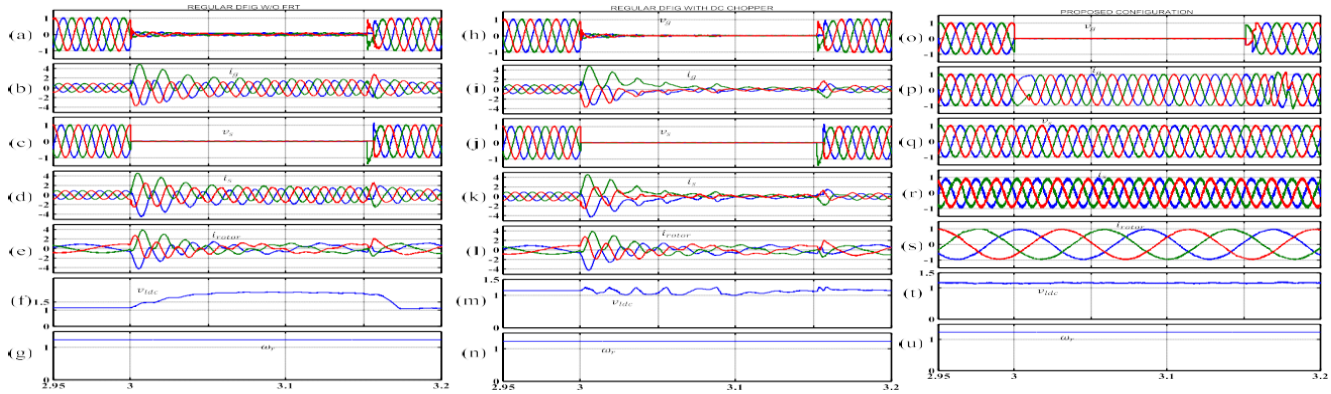

Fig. 9 (a)–(g) Operation of regular DFIG without FRT, (h)–(n) operation of DFIG with DC chopper installed and (o)–(u) operation of proposed configuration

V. CONCLUSION

In this paper, an efficient control strategy is proposed by considering G2V and V2G mode along with reactive power compensation incorporating EVs as an active element safety measures. The developed control algorithm operates satisfactorily in different operating states and the modes of operation are well executed following the power command. The charger has a good steady-state as well as dynamic performance. The off-board charger responds to the power command transition in less than two grid cycles time. The EV battery is not affected during reactive power operation, hence improves battery life. The simulation results validate the proposed controller performance successfully during different power command scenarios. The obtained results show the presented charger is a promising candidate for reactive power support services to be utilized by the utility grid.

REFERENCES

[1] S. S. Williamson, A. K. Rathore and F. Musavi, "Industrial Electronics for Electric Transportation: Current State-of-the-Art and Future Challenges," in IEEE Transactions on Industrial Electronics, vol. 62, no. 5, pp. 3021-3032, May 2015.
[2] A. Kuperman, U. Levy, J. Goren, A. Zafransky, and A. Savernin, “Battery charger for electric vehicle traction battery switch station,”IEEE Trans. Ind. Electron., vol. 60, no. 12, pp. 5391–5399, 2013.
[3] M. Restrepo, J. Morris, M. Kazerani and C. A. Cañizares, "Modeling and Testing of a Bidirectional Smart Charger for Distribution System EV Integration," IEEE Transactions on Smart Grid, vol. 9, no. 1, pp. 152-162, Jan. 2018.
[4] A. Khaligh and S. Dusmez, "Comprehensive Topological Analysis of Conductive and Inductive Charging Solutions for Plug-In Electric Vehicles," IEEE Transactions on Vehicular Technology, vol. 61, no. 8, pp. 3475-3489, Oct. 2012
[5] S. E. Letendre and W. Kempton, “The V2G concept: a new model for power?” Public Utilities Fortnightly, pp. 16–26, Feb. 2002.